Towards a molecular mechanism underlying mitochondrial protein import through the TOM-TIM23 complex

Holly C. Ford, William J. Allen, Gonçalo C. Pereira*, Xia Liu, Mark S. Dillingham and Ian Collinson†

School of Biochemistry, University of Bristol, Bristol BS8 1TD, UK

†, corresponding author: ian.collinson@bristol.ac.uk

*, present address: *MRC - Mitochondrial Biology Unit, University of Cambridge, The Keith Peters Building, Cambridge Biomedical Campus, Cambridge CB2 0XY, UK*

ABSTRACT

Mitochondria contain over a thousand different proteins, which, aside from a few encoded on the mitochondrial genome, are translated in the cytosol and targeted for import. For the majority, the first port of call is the translocase of the outer membrane (TOM-complex); their onward journey is *via* a procession of alternative molecular machines, conducting transport to their final sub-compartment destination: the outer-mitochondrial membrane (OMM), inner-mitochondrial membrane (IMM), inter-membrane space (IMS) or matrix. The pre-sequence translocase of the inner-membrane (TIM23-complex) is responsible for importing proteins with cleavable pre-sequences, and comes in two distinct forms: the $TIM23^{SORT}$ complex mediates IMM protein insertion and the $TIM23^{MOTOR}$ complex is responsible for matrix import. Progress in understanding these transport mechanisms has, until recently, been hampered by the poor sensitivity and time-resolution of import assays. However, with the development of an assay based on split NanoLuc luciferase, we can now explore this process in greater detail. Here, we apply this new methodology to understand how $\Delta\psi$ and ATP hydrolysis, the two main driving forces for transport through the $TIM23^{MOTOR}$ complex, contribute to the import of pre-sequence-containing precursors (PCPs) with varying properties. Notably, we found that two major rate limiting steps define the PCP import time: passage of the PCP across the OMM and initiation of IMM transport by the pre-sequence. The rates of these steps are influenced by PCP properties such as size and net charge, but correlate poorly with the total amount of PCP imported – emphasising the importance of collecting rapid kinetic data to elucidating mechanistic detail. Our results also indicate that PCPs spend very little time in the TIM23 channel – presumably rapid success or failure of import is critical for maintaining mitochondrial health.

INTRODUCTION

Mitochondria are eukaryotic organelles responsible for the biosynthesis of ATP and many other essential cellular functions: biosynthesis of fatty acids (Nowinski et al., 2018) and Fe-S clusters (Rouault, 2012), calcium regulation (Nicholls, 1978), generation of reactive oxygen species (ROS) (Chen et al., 2003)(Nishikawa et al., 2000), intracellular signalling (Hoth et al., 1997)(Chandel, 2015), and apoptosis (Wang and Youle, 2009). Owing to their double-membrane, mitochondria comprise four distinct compartments: the outer-mitochondrial membrane (OMM), inter-membrane space (IMS), inner-membrane (IMM), and matrix. The IMM is highly specialised for the chemiosmotic mechanism of aerobic respiration; it is impermeable to ions and maintains an electrochemical gradient of protons (acidic and positive on the IMS side) – the proton-motive force (PMF). This serves as a form of potential energy, composed of an electrical ($\Delta\psi$) and a chemical (ΔpH) component, used to drive the rotary mechanism of ATP synthesis *inter alia*.

Of more than a thousand proteins that constitute the mitochondrial proteome, all but a handful encoded on the mitochondrial genome (13 in human), are synthesised in the cytosol. A number of bespoke protein import machineries have evolved to transport this highly diverse mixture of soluble and membrane-associated proteins to their various submitochondrial destinations, and for their subsequent folding and assembly into multi-protein complexes. Almost all mitochondrial precursor proteins enter mitochondria *via* the translocase of the outer membrane (TOM complex) which contains the pore-forming β-barrel protein, Tom40. The TOM complex in *Saccharomyces cerevisiae* is thought to form dimers, and possibly trimers and tetramers, and notably their pores have highly negatively charged inner surfaces (Tucker and Park, 2019)(Araiso et al., 2019).

Roughly 60-70% of mitochondrial precursor proteins – almost all those targeted to the matrix and a subset of IMM proteins – have a positively-charged, amphipathic α-helical pre-sequence, also known as a mitochondrial targeting sequence (MTS) (Araiso et al., 2019)(Vögtle et al., 2009). These pre-sequence-containing precursors (PCPs) are transferred to the translocase of the inner membrane (TIM23-complex) once their N-termini emerge from the Tom40 channel, and pass through in an unfolded state (Eilers and Schatz, 1986)(Matouschek et al., 1997)(Neupert and Brunner, 2002)(Rassow et al., 1990) (Neupert and Herrmann, 2007). Genetic and biochemical

experiments have elucidated the key constituents of the TIM23-complex (Blom et al., 1993) (Maarse et al., 1992) (Emtage and Jensen, n.d.) (Maarsea et al., 1994): the core ($TIM23^{CORE}$) comprises three membrane-spanning proteins: Tim23, Tim17 and Tim50. Tim23 is the channel-forming protein and has 4 trans-membrane α-helices (TMH) and a hydrophilic N-terminal region projecting into the IMS which can bind to pre-sequences. Tim17 is required by Tim23 for structural integrity, while the large IMS domain of Tim50 provides the main receptor for PCPs. $TIM23^{CORE}$ associates with different proteins to form complexes tailored to different tasks: together with Tim21 and Mgr2 it forms the $TIM23^{SORT}$ complex, capable of lateral release of proteins with hydrophobic sorting sequences, while association with the pre-sequence translocase-associated motor (PAM) forms the $TIM23^{MOTOR}$ complex, responsible for matrix import. After crossing the IMM, either way, the MTS is cleaved by a matrix processing peptidase (MPP) (Vögtle et al., 2009).

Both pathways into and across the IMM have been shown to require the electrical component of the PMF, the membrane potential ($\Delta\psi$), for transport – as an electrophoretic force on the positively charged pre-sequence (Martin et al., 1991)(Geissler et al., 2000)(Truscott et al., 2001). $\Delta\psi$ alone is sufficient for insertion of membrane proteins *via* the $TIM23^{SORT}$ complex (Callegari et al., 2020), but complete import into the matrix by the $TIM23^{MOTOR}$ complex requires an additional driving force – ATP hydrolysis by the main component of PAM, the mtHsp70 protein (Ssc1 in yeast)(Wachter et al., 1994). The remaining proteins belonging to PAM facilitate its dynamic assembly at the matrix face of the import channel and ensure tight regulation of the ATPase activity of mtHsp70. $\Delta\psi$ has also been implicated in other aspects of $TIM23^{MOTOR}$-mediated PCP import. It promotes Tim23 dimerisation (Bauer and Sirrenberg, 1996), necessary for PCP binding, and is required for Tim17-mediated opening of the channel, which in turn allows the recruitment of Hsp70 by Tim44 (S et al., 2007)(Demishtein-Zohary et al., 2017)(Ting et al., 2017)(Ramesh et al., 2016).

Our basic understanding of the mechanism of protein import *via* the TOM-$TIM23^{MOTOR}$-complex is summarised in Fig. 1A. The unfolded or chaperone-bound PCP binds to the TOM receptor, Tom20, in the OMM. This is followed by sequential: threading and passage of the PCP through the Tom40 channel, transfer to the TIM23 complex in the IMS/ IMM, $\Delta\psi$-dependent translocation

of the pre-sequence into the matrix, and ATP-dependent translocation of the remainder of the protein. This model is primarily derived from end point measurements from a classical import assay involving autoradiography or Western blotting. However, this method is highly limited in its time resolution, and insufficient to provide a deep understanding of the individual steps that make up transport, or their relative contributions to its kinetics. For this reason, we recently developed a highly time-resolved and sensitive assay which exploits a split NanoLuc enzyme (Pereira et al., 2019) to measure protein transport across membranes (Fig. 1B).

In the NanoLuc assay, PCPs tagged with a small fragment of the NanoLuc enzyme (an 11 amino acid peptide called pep86), are added to mitochondria isolated from yeast engineered to contain a matrix-localised large fragment of the enzyme (the enzyme lacking a single beta strand, called 11S). When the PCP-pep86 fusion protein reaches the matrix, pep86 binds rapidly and with tight affinity to 11S forming a complete NanoLuc luciferase. In the presence of the NanoLuc substrate (furimazine), this generates a luminescence signal proportional to the amount of NanoLuc formed. Luminescence is thus a direct readout of the amount of PCP that has entered the matrix, up to the total amount of 11S. As expected, it is $\Delta\psi$-dependent, affected by depletion of ATP, and sensitive to specific inhibitors of TIM23-dependent protein import (Pereira et al., 2019).

Here, we have used the NanoLuc translocation assay to obtain precise, time-resolved measurements of protein delivery into the matrix mediated by the TOM and TIM23^{MOTOR} complexes. To add mechanistic detail to the above model (Fig. 1A), we systematically varied the length and charge of the mature sequences of PCPs and profiled their import kinetics. To better understand the cause of any observed effects on amplitude, rate and lag, we performed experiments under conditions where either of the two main driving forces, $\Delta\psi$ or ATP, had been depleted. Our results suggest that IMM transport itself is fast in normally functioning mitochondria, and limited by the availability of $\Delta\psi$. Analyses such as these, together with emerging structures of the import machinery (Tucker and Park, 2019), will be fundamental to understanding the underlying molecular basis of mitochondrial protein import.

RESULTS

Basic characterisation of protein import suggests under experimental conditions the reaction is largely single turnover

An exemplar NanoLuc import trace is shown in Fig. 1C, collected using the model yeast matrix protein Acp1 (used in previous import studies as a matrix-targeted precursor (Wurm and Jakobs, 2006)) fused to a pep86 (Acp1-pep86). The most intuitive parameter of this trace is amplitude, which corresponds to the amount of NanoLuc formed when the reaction reaches completion, and thus the total number of import events; so long as the pep86 tag does not exceed matrix 11S. In order to verify that this was not the case we estimated the concentration of 11S in the mitochondria by quantitative Western blotting. An antibody raised against 11S was used to compare the quantities of the mitochondrial contained luciferase with known quantities of the purified protein (Fig. S1A). The results reveal high (μM) internal 11S concentrations of with significant variation between mitochondrial preparations (~2.8 - 7.5 μM). We see no correlation between amount of 11S and signal amplitude even with saturating PCP (Fig. S1B-C, and see below). Thus, we conclude that the matrix concentration of 11S is far in excess of the imported PCP, regardless of how much of it is added to the outside.

We next measured signal amplitude over a wide range of concentrations of Acp1-pep86. Plotting the results shows that amplitude is linearly related to PCP concentration up to ~ 45 nM, where it plateaus (Fig. 2A). Because the mitochondrial matrix volume is only ~1/12,000 of the total reaction volume (see Methods), if all 45 nM PCP were imported it would correspond to roughly 540 μM inside the matrix. This is not only far in excess of the internal 11S concentration (as low as ~2.8 μM), but is also implausible simply from the amount of physical space available. Evidently, therefore, only a tiny fraction of the PCP added reaches the matrix.

As neither the amount of PCP added nor the amount of 11S in the matrix appear to be limiting, we next tested to see whether the number of import sites might be having an effect. To estimate the number of import sites, we generated a PCP that can import and give a signal, but which prevents subsequent import events through the same import site – *i.e.* forcing single turnover conditions. To do this, we fused dihydrofolate reductase (DHFR) to the PCP which, in the presence of the inhibitor methotrexate (MTX), folds tightly and cannot be imported (Gold et al., 2017). As expected, if DHFR is positioned N-terminal to pep86 (DHFR-pep86), we see very little

luminescence with MTX present, consistent with blocked import (Fig. 2B). However, when DHFR is positioned C-terminal to pep86 (pep86-DHFR) with sufficient length between the two to span the TOM and TIM complexes (212 amino acids in this case, longer than the 135 required (Rassow et al., 1989)), we do see an import signal (Fig. 2B), confirming that NanoLuc can form as soon as pep86 enters the matrix. Surprisingly, the presence or absence of MTX makes only a minor difference to the amplitude of this signal (Fig. 2B).

Signal amplitude as a function of the pep86-DHFR PCP concentration with or without MTX shows a similar but not identical relationship (Fig. 2C). The slope, which corresponds to the increase in amplitude per 1 nM PCP, is 1.22 times greater in the absence of MTX, meaning only about 20% of the signal arises from turnovers beyond the first. While this does not necessarily mean that import is strictly single turnover – which seems unlikely for fully functional mitochondria – it does suggest that it behaves as single turnover under the reaction conditions here.

Kinetic analysis of import suggests two major rate-limiting steps

In addition to the amplitude data, the import traces contain information about the kinetics of the reaction. Looking again at the data from in Fig. 1C, it can be seen that import does not start at its maximum rate; in most cases there is a lag before transport accelerates. This is characteristic of reactions with multiple consecutive steps, where only the last one gives rise to a signal. As an approximation, the data fit well to a closed equation for a two-step process (see Methods), which gives two apparent rate constants (k_1' and k_2') in addition to amplitude (Fersht, 1984).

In the simplest case possible, where the two steps are irreversible and have very different values, k_1' and k_2' correspond to the two rates for these steps (k_1 and k_2)(Fersht, 1984). This is complicated if the reactions are reversible (in which case the reverse rates also factor), or if k_1 and k_2 are very similar (in which case they are both convoluted into k_1' and k_2'). Nonetheless, this analysis is very useful for understanding the mechanism of import (see below) – especially under conditions where k_1 and k_2 are well separated.

It should be noted that the order of the two steps cannot be determined *a priori*, but we expect the first rate to be dependent on PCP concentration, as association of TOM and PCP is the first step in the transport process. It is also important to note that any additional step faster than about 5 min^{-1} will not be resolved in our experimental set up using deploying a multi-plate reader (Fig. S2A), and will instead manifest as a small apparent lag before the signal appears (equal to $1/k_{step}$, where k_{step} is the rate constant for that process)(Allen et al., 2020). This includes formation of NanoLuc as this is >7.4 min^{-1} even at the lowest estimated 11S concentration, as determined in solution (Fig. S2B). As expected, the internal concentration of 11S does not appreciably affect transport kinetics (Fig. S2C).

Transport is dependent on total protein size

To begin to determine what the two apparent rates correspond to, we first designed and purified two series of four PCPs, varying either in total length or N- to C-terminal positioning of pep86 (Fig. 3A). The length variants all similarly contained the pre-sequence of Acp1 followed by the Acp1 mature domain, with pep86 (L) at the C-terminus. Increase in length was achieved by repeating the mature part of Acp1 up to three times. In between each Acp1 mature domain we included a scrambled pep86 sequence (D), which does not interact with 11S (Allen et al., 2020), such that each tandem repeat has the same overall amino acid (aa) composition. This protein set was designed to reveal potential PCP size-dependence of import. The other set (sequence variants) were all identical to the longest length-variant PCP (four tandem repeats), but with the active pep86 in different positions. Because the sequence variants (abbreviated as LDDD, DLDD, DDLD and DDDL) are identical save for number of aa that must enter the matrix before the NanoLuc signal does, differences in import kinetics between them should reflect processive translocation through the TOM-$TIM23^{MOTOR}$ complex (the ATP-dependent step in Fig. 1A).

Transport of all four length variants (L, DL, DDL and DDDL) and sequence variants (LDDD, DLDD, DDLD and DDDL) at high concentration (1 μM) fit well to the simple two-step model, giving an amplitude and two apparent rate constants (assigned arbitrarily k_1' and k_2') for each. Import traces and the results of fits to the two-step model are plotted in Fig. 3B and C respectively, with error bars representing the SEM from three biological replicates.

For the length series, signal amplitude is inversely correlated with protein length (Fig. 3C). This is not because the PCPs become trapped in the import channel during transport, as the sequence variants all have the same amplitude (Fig. 3C). Instead, it seems that small proteins are able to accumulate at higher levels in the matrix than large ones. This is consistent with the idea that energy depletion limits import – it takes more energy to import a larger protein – rather than a limitation of the amount of 11S, as this would result in the same maximum amplitude for all proteins. In terms of rates, we find that the faster rate constant (k_1') has a strong inverse correlation with PCP length (but not pep86 position), *i.e.* it is faster for smaller proteins, while k_2' shows little effect.

To explore the length and sequence variants further, we measured protein import for both protein sets over a range of PCP concentrations, and fitted the data in the same way (Fig. 4). Just as before, we find no systematic difference between the sequence variants (Fig. 4D-F) – clearly passage of the PCP through TIM is not limiting the overall transport rate. For the length series, however, the apparent K_d for import increases as PCP length increases; effectively, more PCP must be added to produce the maximum amplitude (Fig. 4A), even though that amplitude is lower (Fig. 3B-C). It is difficult to estimate accurate K_Ms for the fitted rate constants as they are hard to assign when they are very similar, but it appears the slow rates (k_2') have approximately the same apparent K_M as amplitude, while the fast rates (k_1') all have a similar apparent K_M, in the low 100s of nM.

Depletion of Δψ has a stronger effect on import than depleting ATP

To better understand the molecular basis for the length-dependence of import, we measured import of the length and sequence variants under conditions in which each of the two driving forces (Δψ and ATP) were depleted. Partial depletion of Δψ by pre-treatment of mitochondria with valinomycin, a potassium ionophore, causes a decrease in signal amplitude for all lengths and sequence variants, affecting them roughly equally (Fig 5A). Intriguingly, valinomycin has very different effects on the two apparent rate constants: k_1' is somewhat slowed for shorter proteins but largely unaffected for longer ones (Fig. 5A), while k_2' is somewhat slowed for short proteins but dramatically reduced for longer ones (Fig. 5A).

Depletion of matrix ATP was achieved simply by excluding ATP and its regenerating system from the assay buffer. Endogenous matrix ATP under these conditions is minimal, as is evident from the fact that import becomes highly sensitive to antimycin A, an inhibitor of oxidative phosphorylation (Fig. S3). This sensitivity arises because ATP is required for hydrolysis by the ATP synthase to maintain $\Delta\psi$ in the absence of oxidative phosphorylation(Campanella et al., 2008). Import experiments performed with depleted ATP show reduced amplitude, but unlike valinomycin this effect is more pronounced for the longer PCPs (Fig. 5B) – consistent with proposed role for ATP in promoting transport of the mature part of the PCP. ATP depletion has little or no effect on k_1', and a relatively minor effect on k_2' (Fig. 5B), affecting both the length and sequence variants roughly equally.

A simple working model for transport based on the above results

Taking all the above observations together, we can propose a simplified model for import that incorporates two major rate-limiting steps. Because k_2' is somewhat sensitive to ATP, it most likely comes at the end of transport, as the contribution of Hsp70 requires at least some of the PCP to be in the matrix. Since k_2' shows very little dependence on PCP length in fully energised mitochondria, we propose that it is primarily the $\Delta\psi$-dependent insertion of the pre-sequence through TIM23, not the subsequent passage of the unfolded passenger domain that is limiting (although both presumably contribute the apparent rate constant). However, under conditions of $\Delta\psi$ depletion, a length-dependence of k_2' emerges: this is consistent with import rate of the rest of the PCP being affected by $\Delta\psi$ ((Schendzielorz et al., 2017), and see also below). It is also possible that transport of longer PCPs has a higher chance of failure, with the PCP slipping back into the IMS – this would be a useful mechanism to prevent TIM23 complexes becoming blocked with defective PCPs, and would explain the difference in the effect of $\Delta\psi$ depletion on the length and sequence variants.

The other apparent rate constant, k_1', is strongly dependent on PCP concentration (Fig. 4), however this saturates with an apparent K_M of around 100-200 nM. This is indicative of a two-step process, where the first is PCP binding and dissociating in rapid equilibrium (too fast to measure as a step in itself), followed by a slower step that proceeds from the bound form:

$$PCP + TOM \underset{k_{off}}{\overset{k_{on}}{\rightleftarrows}} TOM.PCP \overset{k_1}{\rightarrow} TOM.PCP^{*}.$$

The strong dependence of k_1' on PCP length provides a clue as to the nature of k_1 – it is likely to correspond to passage of the PCP across the OM, through the TOM complex.

Putting all of this together, we propose the following minimal kinetic scheme for PCP import:

$$PCP_{out} + TOM \underset{k_{off}}{\overset{k_{on}}{\rightleftarrows}} TOM.PCP_{out} \overset{k_1}{\rightarrow} TOM.PCP_{IMS} \overset{k_2}{\rightarrow} PCP_{in},$$

where the subscript to PCP indicates its location (outside the OM, in the IMS, or inside the matrix). In this model, k_{on} and k_{off} are both fast compared with k_1, and give an affinity ($K_d = k_{off}/k_{on}$) in the order of 100 nM, similar to the affinity (~ 35 nM) of a bacterial secretion preprotein to bacterial inner membrane vesicles (Hartl et al., 1990). The two extracted rate constants can be approximately determined as ([PCP] designates PCP concentration):

$$k_1' \sim k_1 \frac{[PCP]}{K_d + [PCP]} \quad \text{and} \quad k_2' \sim k_2$$

This model fits the data, and we believe it is the most reasonable interpretation of the above experimental results. However it still leaves open several questions, notably the extent to which k_1 and k_2 are reversible. For example, the fact that k_1' is somewhat affected by valinomycin (Fig. 5A) suggests that k_1 is to some extent reversible, given that passage through TOM can occur in the absence of $\Delta\psi$ (Mayer et al., 1993)(Lill et al., 1992): slowing k_2 would then leave more opportunity diffusion back out of the IMS through TOM, a process that occurs in the absence of ATP (Ungermann et al., 1996). In addition, we cannot determine from this data exactly at what stage handover from TOM to TIM23 occurs, whether the entire PCP must pass through TOM first, or even whether it can dissociate from TOM before binding to TIM23.

Changing PCP net charge affects import amplitude and rate differently

$\Delta\psi$, the electrical component of the PMF (positive outside), has been proposed to act primarily upon positively charged residues in the PCP, pulling them through electrophoretically (Martin et

al., 1991)(Geissler et al., 2000)(Truscott et al., 2001). To test this idea, we designed a series of proteins, based on a engineered version of the N-terminal section of yeast cytochrome b_2 lacking the stop-transfer signal (Δ43-65) to enable complete matrix import (Gold et al., 2014), with varying numbers of charged residues (Fig. 6A). These proteins were of the same length, but spanned 5.43 units of pI ranging from 4.97 to 10.4. Import of these charge variants under saturating conditions (1 μM PCP) was measured using the NanoLuc assay as above (Fig. 6B).

The most immediately striking observation is that amplitude is strongly *inversely* correlated with net charge of the PCP – *i.e.* the opposite of what might be expected given the direction of Δψ (Fig. 6C). To understand why this would be, we turned to our earlier interpretation of signal amplitude: that it is limited by the availability of Δψ. If transport of positively charged residues depletes Δψ while transport of negatively charged residues replenishes it, this could explain why negatively charged proteins accumulate to a higher level.

To test this hypothesis, we monitored Δψ in isolated mitochondria over time by measuring TMRM fluorescence, then assessed the effect of adding the PCPs with differing net charge (Fig. 6D). The PCPs did indeed cause strong depletion of Δψ and, moreover, this effect diminished with increasing net negative charge. Increasing net positive charge did not seem to result in enhanced depletion of Δψ, but TMRM does not resolve Δψ well in this range, so this does not necessarily mean that this effect is not occurring. A second prediction from this hypothesis is that membrane depolarisation prior to protein import will abolish the correlation between net charge and amplitude. This is indeed exactly what we see: valinomycin reduces amplitudes for all PCPs, but the effect is greater for more negatively charged PCPs, bringing all amplitudes to about the same level (Fig. 6E). Depleting ATP, meanwhile, has very little effect on amplitude, just as for the Acp1-based PCPs.

Looking at the import traces for the charge series, it is clear that positively charged PCPs are imported much faster than negatively charged ones (albeit reaching a lower final amplitude; Fig. 6B-C). This is again consistent with Δψ specifically assisting the transport of positively charged residues. Unlike the length variants based on Acp1, however, not all of the import traces from the charge variants fit to the two step model (Fig. 6B). While the more negatively charged ones have

a clear lag before reaching their maximum rate, the positively charged ones appear to have only a single rate-limiting step, or even to have a burst of rapid import, followed by a slower phase (Fig. 6B). Because steps are only resolved on the plate reader if they are ≤ about 5 min^{-1}, the most likely explanation for this is that one phase has become too fast to measure. This is most likely transport through TIM23, which is strongly Δψ-dependent and thus presumably faster for more positively charged proteins. A burst suggests multiple turnovers, with the first one very fast, and subsequent ones limited by a slower resetting of TIM23 (see Discussion).

Testing the above results with native PCPs

While the use of artificial PCPs, as above, allows their properties to be varied in a systematic manner, it is possible that these modifications will affect native features with fundamental roles in the import process. To confirm that the above observations hold true for native PCPs we performed import experiments with four pep86-tagged native PCPs differing in length and charge. We chose the F_1 α and F_1 β subunits of the mitochondrial ATP synthase, both large proteins (>500 amino acids) with mature amino acid sequences differing in predicted pI by ~ 1.55 (F_1 β = 5.43 and F_1 α = 6.98); and two smaller proteins (<200 amino acids), Acp1 and Mrp21, with predicted mature sequence pIs of 4.87 and 10.00 respectively (Fig. 7A).

Consistent with our earlier results, we see higher amplitudes for the shorter and more negatively charged PCPs (Fig. 7B), and faster transport of the shorter PCPs than the longer ones (Fig. 7B). The effect of net charge holds true for the larger PCPs, which both have clear two-step transport (Fig. 7B), but the small PCPs appear to have only a single rate-limiting step, and do not differ significantly in import rate (Fig.7B). Presumably the charge dependence only becomes measurable when transport through TIM23 is slow enough to be appreciable. Overall, these results suggest that the data collected with artificial PCPs will hold true for native ones as well.

DISCUSSION

Protein import into mitochondria is, by nature, a complicated process with machineries in two membranes having to coordinate with one another as well as with parallel import pathways to deliver a wide range of proteins to their correct destinations. Here, we have built a basic

mechanistic model of one of the major import routes – the TOM-TIM23^{MOTOR} pathway of matrix proteins – using a high-resolution import assay based on NanoLuc. Our results suggest that two major events are responsible for the majority of the PCP transit time: passage of the PCP through the TOM complex and initiation of import by insertion of the pre-sequence through the TIM23^{MOTOR} complex. By contrast, the initial binding of PCP to TOM is fairly rapid, as is passage of the mature PCP domain through TIM23. Crucially, the rates of the different steps correlate very poorly with the amount of PCP in the matrix when the reaction ends, which has always been the conventional readout of import. It therefore seems that this pre-steady-state kinetic approach will be critical in the future, both for further dissecting import via the TOM-TIM23^{MOTOR} complex and for understanding the other pathways that together comprise the mitochondrial protein import machinery.

Import appears to be largely single turnover under our experimental conditions, that is each import site only imports a single PCP. While this is fortuitous in that it allows us to access pre steady-state events easily, it is incongruent with mitochondrial protein import *in vivo*. We propose that, under experimental conditions, transport is limited by the amount of energy available in the form of $\Delta\psi$. Indeed, measurements of $\Delta\psi$ using TMRM confirm that PCP import causes a depolarisation of the IMM that is not restored. Also consistent with $\Delta\psi$ being consumed, we find that the PCPs that require more total energy to import (such as longer ones), or that are likely to consume more $\Delta\psi$ (positively charged ones) reach a lower concentration in the mitochondrial matrix. The mechanism by which $\Delta\psi$-depletion leads to single turnover conditions is likely to relate to the requirement of $\Delta\psi$ for dimerization of TIM23 and recruitment of Tim44, both required for delivery to the matrix. As PCPs bind only to dimeric TIM23 complexes and, during transport, disrupt this conformation, loss of $\Delta\psi$ would prohibit the resetting of the TIM23 complex to allow turnovers after the first (Bauer and Sirrenberg, 1996). With some of the faster transporting PCPs we do indeed see a rapid burst of import followed by a slower phase, as would be expected for multiple turnovers where the first is fast. This could therefore provide a window for future studies to investigate this priming event.

Previous studies have shown that the TOM-complex is in excess over TIM23, with 1 mg yeast mitochondria containing ~17-20 pmol TIM23 (~9-10 pmol dimer) and estimations of between 85

and 250 pmol TOM40 (Sirrenberg et al., 1997)(Dekker et al., 1997). In our experiments, this TIM23 dimer concentration equates to ~62.5 fmol per well (10 $pmol.mg^{-1}$ × 50 $\mu g.ml^{-1}$ × 125 µl) – similar to the estimated amount of 11S (~28-76 fmol per well, based on an estimated 4.46-12.17 $pmol.mg^{-1}$). This close correspondence presumably explains why we find that 11S is not limiting, but intriguingly, it also suggests that each import site only imported on average one 11S, even though 11S import occurred in live yeast before mitochondrial isolation. This correspondence may not be coincidental; if the number of TIM23 sites limited import, this could be calibrated as a regulatory mechanism to avoid proteotoxic stress.

The transfer of PCPs from TOM to TIM23 is thought to involve cooperative interactions of subunits of the two complexes (Callegari et al., 2020). But the extent to which transport of PCPs across the OMM and IMM is coupled, remains unknown. It has been suggested that the rate of PCP passage through the OMM is one factor that determines whether PCPs are transferred to the matrix or released laterally into the IMM (Harner et al., 2011), implying simultaneous and cooperative activities of TOM and TIM23. PCPs have been captured spanning both membrane complexes at the same time in super-complexes of ~600 kDa (Dekker et al., 1997)(Gold et al., 2014)(Chacinska et al., 2010). Moreover, it has been proposed that Tim23 has a topology spanning the OMM as well as the IMM, with its N-terminus domain exposed on the cytosolic face of the OMM, and is thus thought to act as a tether (Donzeau et al., 2000), presumably increasing import efficiency. These proximal associations of TOM and TIM23 suggest that import through TOM does not have to be complete before import through TIM23 can begin.

However, there is also evidence to suggest that the TOM and TIM23 complexes can transport PCPs independently, in steps that are not necessarily concurrent. Matrix import of PCPs has been observed in mitoplasts (Hwang et al., 1989)(Ohba and Schatz, 1987), in which the OMM has been removed, suggesting that a handover from TOM is not absolutely required. The *in vivo* existence of TOM-TIM23 super-complexes is unconfirmed. They have been detected only when engineered PCPs with C-terminal domains that cannot pass through TOM are used (Chacinska et al., 2003). And only under these artificial conditions do TOM and TIM23 subunits co-immuno-precipitate (Horst et al., 1995). Their assembly must be dynamic and transient. Moreover, the N-terminal

domain of Tim23, that tethers the IMM and OMM, is not required for either PCP import though TIM23, or TOM-TIM23 super-complex formation (Chacinska et al., 2003).

Our results also hint that this handover is not absolutely required. The data here suggest that transport of a PCP through TOM is reversible, and therefore possible in the absence of TIM23 activity. Reverse transport of proteins through TOM, and in some cases also through TIM23, has been observed previously, although this process is not well understood. Proteins that are reduced or conformationally unstable in the IMS can retro-translocate to the cytosol *via* TOM40, and the efficiency of this process is relative to protein size (both linear length and 3D complexity); smaller proteins are more efficiently retro-translocated (Bragoszewski et al., 2015). Under physiological conditions, PINK1 is cleaved in the IMM by PARL, releasing the remaining C-terminal region for release back to the cytosol for proteosomal degradation. But the process is not well understood, such as if, and how, it is regulated, and if a driving force is required. Additionally, we see some PCP concentration dependence of k_2'; if direct interaction of TOM with TIM23 were strictly required then k_2 would not be affected by PCP concentration, but if PCP can accumulate in the IMS this would explain our finding.

Overall, the above analysis provides good estimates of the two rate limiting steps for import, and provides evidence as to the constraints that act upon the others. If a few of the above questions are resolved, we believe it should be possibly to construct a complete kinetic model of mitochondrial import, as has been recently achieved for the bacterial Sec system (Allen et al., 2020).

MATERIALS AND METHODS

Strains and plasmids

E. coli α-select cells were using for amplifying plasmid DNA and BL21 (DE3) used for protein expression. Genes encoding pep86 tagged mitochondrial PCP proteins were cloned into either pBAD or pRSFDuet. YPH499 yeast cells transformed with pYES2 containing the mt-11S gene under control of the GAL promoter, were used for isolation of mitochondria containing matrix-localised 11S. *E. coli* cells were routinely grown at 37°C on LB agar and in either LB or 2XYT medium containing appropriate antibiotics for selection. Yeast cells were grown at 30°C on

synthetic complete dropout agar supplemented with 2% glucose, penicillin and streptomycin, or in synthetic complete dropout medium, supplemented with 3% glycerol, penicillin and streptomycin in baffled flasks. For yeast cells with mitochondrial matrix-localised 11S, mt-11S was expressed by adding 1% galactose at mid-log phase, 16 hours prior to harvesting of cells.

Protein production and purification

BL21 (DE3) cells from a single colony, containing the chosen protein expression plasmid were grown in LB overnight then sub-cultured in 2XYT medium until OD_{600} reached 0.6. Protein expression was induced by adding arabinose or IPTG, for pBAD and pRSFDuet plasmids respectively. Cells were harvested 2-3 hours later and lysed using a cell disrupter. Proteins were purified from inclusion bodies using Nickel affinity chromatography on prepacked HisTrap FF columns (Cytiva), followed by ion exchange chromatography on either HiTrap Q HP or HiTrap SP HP columns (Cytiva) depending on protein charge, described in full previously (Pereira et al., 2019).

Isolation of mitochondria from yeast cells

Yeast cells were harvested by centrifugation (4,000 x g, 10 min, room temperature) and mitochondria isolated by differential centrifugation (Daum et al., 1982). Briefly, cell walls were digested with zymolyase in phosphate-buffered sorbitol (1.2 M sorbitol, 20 mM potassium phosphate pH 7.4), after being reduced with DTT (1 mM DTT in 100 mM Tris-SO4 at pH 9.4, for 15 min at 30°C). Cells were disrupted at 4°C with a glass Potter-Elvehjem homogeniser with motorised pestle in a standard homogenisation buffer (0.6 M sorbitol, 0.5% (w/v) BSA, 1 mM PMSF, 10 mM Tris-HCl pH 7.4). The suspension was centrifuged at low speed (1,480 x *g*, 5 min) to pellet unbroken cells, cell debris and nuclei, and mitochondria harvested from the supernatant by centrifugation at 17,370 x *g*. The pellet, containing mitochondria, was washed in SM buffer (250 mM sucrose and 10 mM MOPS, pH 7.2), and then centrifuged at low speed again, to remove remaining contaminants. The final mitochondrial sample, isolated from the supernatant by centrifugation (17,370 x *g*, 15 min), was resuspended in SM buffer and protein quantified by bicinchoninic acid (BCA) assay (Smith et al., 1985) using a bovine serum albumin protein standard. Mitochondria were stored at -80°C, at a concentration of at 30 mg/ml in single use aliquots, after being snap frozen in liquid nitrogen.

NanoLuc import assay

Unless stated otherwise, import experiments were performed at 25°C with mt-11S mitochondria diluted to 50 µg/ml in import buffer (250 mM sucrose, 80 mM KCl, 1 mM K_2HPO_4/KH_2PO_4, 5 mM $MgCl_2$, 10 mM MOPS-KOH and 0.1% (v/v) Prionex reagent (Merck), pH 7.2), supplemented with 2 mM NADH, 1 mM ATP, 0.1 mg/ml creatine kinase, 5 mM phosphocreatine, and 1 µM pep86-tagged PCP protein. We also added 10 µM GST-Dark protein; a fusion of glutathione S-transferase and a peptide with high affinity for 11S, that inhibits pep86 binding and concomitant enzymatic activity, and thereby reduces background signal caused by trace amounts of 11S outside of the mitochondrial matrix. Mitochondria and GST-Dark were added to 1X import buffer at 1.25X final concentrations (mixture 1), and pep86-tagged PCP protein, NADH, ATP, creatine kinase and phosphocreatine added to 1X import buffer at 5X final concentrations (mixture 2) so that import reactions could be started by the injection of 4 vols mixture 1 onto 1 vol mixture 2. In selected experiments, depletion of $\Delta\psi$ was achieved by pre-treating mitochondria for 5 minutes with 10 nM valinomycin, and depletion of ATP was achieved by omitting ATP, creatine kinase and phosphocreatine from the reaction. Luminescence was read from 125 µl reactions in a white round-bottom 96 well plate (Thermo Scientific) on either a CLARIOStar Plus (BMG LABTECH), or a BioTek Synergy Neo2 plate reader (BioTek Instruments) without emission filters. The mitochondrial matrix volume as a fraction of reaction volume was estimated using the previously published yeast mitochondrial matrix volume of 1.62±0.3 µl/mg (Koshkin and Greenberg, 2002). Thus when mitochondria are at 50 µg/ml, matrix volume will be 81±15 nl/ml, or ~1/12345.68 total volume (between 1/15151.5 and 1/10416.7 accounting for error).

Data processing and analysis

NanoLuc assay data were processed using a combination of software: Microsoft Excel, pro Fit and GraphPad Prism. Data were then normalised to the maximum luminescence measurement for each experiment.

In most cases, the resulting data were fitted using pro Fit to a model for two consecutive, irreversible steps, where the final one gives rise to a signal (Fersht, 1984):

$$Y = A_0\left(1 + \frac{1}{k_1 - k_2}\left(k_2 e^{-k_1 t} - k_1 e^{-k_2 t}\right)\right),$$

where A_0 is amplitude, k_1 and k_2 the two rate constants, Y the signal and time. Note that this equation produces the same result whichever order k_1 and k_2 are in. Subsequent analyses of the resultant data were done in GraphPad Prism; linear and non-linear (Michaelis-Menten) regression.

Membrane potential measurements with isolated mitochondria

Isolated mitochondria were diluted to 50 µg/ml in import buffer (described above) supplemented with 1 mM ATP, 0.1 mg/ml creatine kinase, 5 mM phosphocreatine, 10 µM GST-Dark protein and 0.5 µM Tetramethylrhodamine methyl ester (TMRM). Relative $\Delta\psi$ was monitored over time as a change in fluorescence of the $\Delta\psi$-dependent dye TMRM in quenching mode. Fluorescence was measured at an excitation wavelength of 548 nm and an emission wavelength of 574 nm, in black plates, on a BioTek Synergy Neo2 plate reader (BioTek Instruments). The inner membrane PMF was generated by injecting 2 mM NADH, and PCP proteins added manually after stabilisation of fluorescence.

Acknowledgments:

We would like to thank Prof. Andrew Halestrap for his insight and enthusiastic discussions on the mysteries of mitochondrial bioenergetics. We also thank past and present members of the Collinson lab who helped to get this project off the ground, particularly Drs Andrew Richardson and Dylan Noone.

Funding:

This research was funded by the Wellcome Trust: Investigator Award to IC (104632/Z/14/Z).

Author contribution:

Project conceptualisation: GCP, HCF and IC

Sample preparation: HCF and XL

Data Collection: HCF

Data Analysis: HCF and WJA

Data interpretation: HCF, WJA and MSD

Manuscript writing: HCF, WJA and IC

Funding acquisition and project management: IC

Declarations:

The authors declare no competing interests. The funding agency and the University had no role in study design, data collection and analysis, decision to publish, or preparation of the manuscript. For the purpose of Open Access, the author has applied a CC BY public copyright licence to any Author Accepted Manuscript version arising from this submission.

FIGURE LEGENDS:

Figure 1: Model of PCP import into mitochondria and outline of the NanoLuc import assay

A) Simple model of presequence-containing precursor (PCP) import into mitochondria, showing binding of PCP to the TOM complex, Δψ-dependent movement of the presequence into the matrix, ATP-dependent translocation of the remainder of the protein, and binding of the C-terminal pep86 to 11S which forms NanoLuc in the matrix.

B) Diagramatic representation of the NanoLuc real-time import assay.

C) An example of luminescence data from the NanoLuc import assay, showing the fit to a model for two consecutive, irreversible steps (see Methods).

Figure 2: Basic characterisation of PCP import and turnover number

A) The effect of varying PCP concentration (Acp1-pep86) on signal amplitude. A straight line was fitted to the data where amplitude increased linearly with PCP concentration (red), and to the data where amplitude increased only marginally (blue). The intersect of these lines and corresponding PCP concentration, the point of plateau, is also shown (purple).

B) The effect of MTX on signal amplitude of three proteins (depicted schematically below): Acp1-DHFR-pep86 (purple), where MTX prevents entry of pep86; Acp1-pep86-DHFR (orange), where MTX limits import to one pep86 per import site; and Acp1-pep86 (grey), for which MTX should have no effect. Bars show the average and SEM from three independent biological replicates.

C) Signal amplitude as a function of Acp1-pep86-DHFR concentration in the absence (solid circles) and presence (open circles) of MTX.

Figure 3: Using proteins of varying lengths to elucidate import kinetics

A) Schematic of two protein series (length variants and sequence variants), with MTS in grey, mature Acp1 in red, pep86 in yellow (L for light) and scrambled pep86 in blue (D for dark).

B) Example of import traces for length variants (left panel) and sequence variants (right panel). Error bars show SD from biological triplicate, each conducted in duplicate.

C) Parameters obtained from two step fits to the data shown in panel B. The length series is shown in orange and the sequence series in teal. Error bars show SEM from biological triplicate, each conducted in duplicate.

Figure 4: The concentration dependence of length and sequence variants

A-F) Amplitudes (**A, D**), k_1', assigned as the faster rate (**B, E**) and k_2' (**C, F**) for the length (**A-C**) and sequence (**D-F**) series, coloured red, orange, yellow and green in order of increasing length or pep86 position. All individual fits from 4-6 independent biological replicates of each set are shown, and the secondary data are fitted to the Michaelis-Menten equation, with errors estimated from the fitting.

Figure 5: Effects of energy depletion on transport of the length and sequence variants

A) Transport without (solid circles) or with (open circles) depletion of $\Delta\psi$, for the length (orange) and sequence (teal) series. Plots show amplitude (left), k_1' (middle) and k_2' (right) extracted from two-step fits to import traces as a function of PCP length or pep86 position. Each point is the average and SEM of three independent biological replicates.

B) As in panel A, but without (solid circles) or with (open circles) ATP depletion instead of valinomycin.

Figure 6: The effect of PCP charge on import kinetics

A) Overview of the charge variant protein series, showing numbers of positively (blue) and negatively (red) charged residues, and symbols for each protein with colours corresponding to theoretical pI, according to the scale shown on the left.

B) Import traces for the charge variant proteins in which the number of negative (left) and positive (right) charges are varied, normalised to the native PCP, coloured by rainbow from most negative (red) to most positive (violet). Data shown are a single representative trace; this is because starting points for each data set are slightly offset due to the injection time of the plate reader. Full data – three biological replicates each performed in duplicate – are shown in Fig. S4A.

C) Amplitudes obtained from panel (**B**) as a function of net charge (coloured as in panel B), with a line of best fit shown.

D) TMRM fluorescence over time with isolated yeast mitochondria (left), with PCPs added at the time indicated by arrowhead. A no protein control (buffer only) is shown in grey, and the remaining traces are shown with the PCP coloured as in panel B. Average TMRM fluorescence over a 5 minute window (between orange lines) was calculated for each trace then plotted, relative

to no protein control, against protein net charge (right). Data shown is mean ± SD from three biological repeats.

E) Amplitude (normalised to the native PCP in standard conditions) of import signal for the charge variants, where numbers of negatively (left) or positively (right) charged residues is varied, under standard reaction conditions (grey) or when $\Delta\psi$ (purple) or ATP (green) is depleted. Each data point is the mean ± SEM from three biological repeats (shown in Fig. S4B-C).

Figure 7: Transport of pep86 fused native precursors

A) Schematic representation of the four native precursors chosen: $F_1\alpha$ (long, positively charged), $F_1\beta$ (long, negatively charged), Mrp21 (short, positively charged) and Acp1 (short, negatively charged).

B) Transport signal for the four proteins in panel A, normalised to Acp1. Each trace is the mean ± SD of three biological repeats.

Figure S1: 11S levels and signal amplitude

A) Western blot against 11S (bottom) and TOM40 (contro1, top) of eight different mitochondrial preparations extracted from four different batches of yeast. 60 µg each sample of mitochondria was fractionated by SDS-PAGE prior to Western blot. Two known concentrations of purified his-tagged 11S are also included for quantification by densitometry.

B) Import traces of Acp1-pep86 with each of the mitochondrial preps in panel **A**, performed in parallel and unnormalised.

C) Signal amplitude from panel **B** as a function of 11S concentration (normalised to TOM40) from panel **A**, with points coloured as in panel **B**. The results show no correlation between 11S concentration and amplitude.

Figure S2: Constraints of data fitting to the NanoLuc import traces.

A) The expected signal for a two-step transport process, with k_2' fixed at 0.5 min^{-1} and k_1' varied between 0.1 min^{-1} (red) and 12.8 min^{-1} (magenta). As k_1' increases, it makes increasingly less difference to the overall shape of the curve. Because the plate reader measures luminescence with a frequency of 10 min^{-1} (represented as vertical gridlines in the zoomed in panel, right), any rate

constants faster than about 5 min^{-1} will not be resolved. The same effect holds true for any additional rates that form part of the mechanism but are faster than ~5 min^{-1}.

B) Amplitude (blue) and rate (green) determined from a single exponential fits to NanoLuc formation is solution. Substrate (pep86) is provided in the form of GST-pep86 which is not a PCP, and 11S comes from mitochondria solubilised completely with digitonin (5 mg/ml) to simulate binding within the mitochondrial matrix. Fits are to the Michaelis Menten equation giving an affinity of 15.6 nM and a v_{max} of 7.4 min^{-1}.

C) The import traces in Fig. S1B all normalised to 1, coloured in the same way. The fact that all the traces overlay well confirms that binding of 11S is too fast to constitute either of the rates extracted from the two step fits – as expected given that the binding rate should be close to v_{max} for NanoLuc formation (as determined in panel **B**).

Figure S3. Confirmation of ATP depletion in the mitochondrial matrix.

Import traces for Acp1-pep86 (left) and Mrp21-pep86 (right) in the presence (filled circles) or absence (open circles) of ATP and its regenerating system, and the absence (red and blue) or presence (orange and lilac) of antimycin A (AA).

Figure S4. Complete import traces for the data in Fig. 6.

A) Two technical repeats each of three biological replicates, under standard conditions.

B) Three biological replicates with $\Delta\psi$ depletion (valinomycin)

C) Three biological replicates with ATP depletion.

REFERENCES:

Allen WJ, Watkins DW, Dillingham MS, Collinson I. 2020. Refined measurement of SecA-driven protein secretion reveals that translocation is indirectly coupled to ATP turnover. *Proc Natl Acad Sci U S A* **117**:31808–31816.

Araiso Y, Tsutsumi A, Qiu J, Imai K, Shiota T, Song J, Lindau C, Wenz LS, Sakaue H, Yunoki K, Kawano S, Suzuki J, Wischnewski M, Schütze C, Ariyama H, Ando T, Becker T, Lithgow T, Wiedemann N, Pfanner N, Kikkawa M, Endo T. 2019. Structure of the mitochondrial import gate reveals distinct preprotein paths. *Nature* **575**:395–401.

Bauer MF, Sirrenberg C. 1996. Role of Tim23 as Voltage Sensor and Presequence Receptor in Protein Import into Mitochondria. *Cell* **87**:33-41

Blom J, Kubrich M, Rassow J, Voos W, Dekker PJT, Maarse AC, Meijer M, Pfanner2 N, Maarse JC, Blom LA, Grivell M, Meijer J. 1993. The Essential Yeast Protein MIM44 (encoded by MPI) Is Involved in an Early Step of Preprotein Translocation across the Mitochondrial Inner Membrane The essential yeast gene MPI1 encodes a mitochondrial membrane protein that is possibly involved in protein. *Mol Cell Biol* **13**:7364–7371.

Bragoszewski P, Wasilewski M, Sakowska P, Gornicka A, Böttinger L, Qiu J, Wiedemann N, Chacinska A. 2015. Retro-translocation of mitochondrial intermembrane space proteins. *Proc Natl Acad Sci U S A* **112**: 7713-7718.

Callegari S, Cruz-Zaragoza LD, Rehling P. 2020. From TOM to the TIM23 complex – handing over of a precursor. *Biol Chem* **401**:709–721.

Campanella M, Casswell E, Chong S, Farah Z, Wieckowski MR, Abramov AY, Tinker A, Duchen MR. 2008. Regulation of Mitochondrial Structure and Function by the F1Fo-ATPase Inhibitor Protein, IF1. *Cell Metab* **8**:13–25.

Chacinska A, Rehling P, Guiard B, Frazier AE, Schulze-Specking A, Pfanner N, Voos W, Meisinger C. 2003. Mitochondrial translocation contact sites: separation of dynamic and stabilizing elements in formation of a TOM–TIM–preprotein supercomplex. *EMBO J* **22**:5370.

Chacinska A, van der Laan M, Mehnert CS, Guiard B, Mick DU, Hutu DP, Truscott KN, Wiedemann N, Meisinger C, Pfanner N, Rehling P. 2010. Distinct Forms of Mitochondrial TOM-TIM Supercomplexes Define Signal-Dependent States of Preprotein Sorting. *Mol Cell Biol* **30**:307–318.

Chandel NS. 2015. Evolution of Mitochondria as Signaling Organelles. *Cell Metab* **22**:204-206.

Chen Q, Vazquez EJ, Moghaddas S, Hoppel CL, Lesnefsky EJ. 2003. Production of reactive oxygen species by mitochondria: Central role of complex III. *J Biol Chem* **278**:36027–36031.

Daum G, Böhni PC, Schatz G. 1982. Import of proteins into mitochondria. Cytochrome b2 and cytochrome c peroxidase are located in the intermembrane space of yeast mitochondria. *J Biol Chem* **257**:13028–13033.

Dekker PJT, Martin F, Maarse AC, Bömer U, Müller H, Guiard B, Meijer M, Rassow J, Pfanner N. 1997. The Tim core complex defines the number of mitochondrial translocation contact sites and can hold arrested preproteins in the absence of matrix Hsp70-Tim44. *EMBO J* **16**:5408–5419.

Demishtein-Zohary K, Günsel U, Marom M, Banerjee R, Neupert W, Azem A, Mokranjac D. 2017. Role of Tim17 in coupling the import motor to the translocation channel of the mitochondrial presequence translocase. *Elife* **6**:e22696

Donzeau M, Káldi K, Adam A, Paschen S, Wanner G, Guiard B, Bauer MF, Neupert W, Brunner M. 2000. Tim23 links the inner and outer mitochondrial membranes. *Cell* **101**:401–412.

Eilers M, Schatz G. 1986. Binding of a specific ligand inhibits import of a purified precursor protein into mitochondria. *Nature* **322**:228–32.

Emtage JLT, Jensen RE. 1993. MAS6 Encodes an Essential Inner Membrane Component of the Yeast Mitochondrial Protein Import Pathway. *The Journal of Cell Biology* **122**:1003-1012.

Fersht A. 1984. Enzyme Structure and Mechanism.

Geissler A, Krimmer T, Bö mer U, Guiard B, Rassow J, Pfanner N. 2000. Membrane Potential-Driven Protein Import into Mitochondria The Sorting Sequence of Cytochrome b 2 Modulates the-Dependence of Translocation of the Matrix-targeting Sequence. *Molecular Biology of the Cell* **11**:3977-3991

Gold VA, Chroscicki P, Bragoszewski P, Chacinska A. 2017. Visualization of cytosolic ribosomes on the surface of mitochondria by electron cryo-tomography. *EMBO Rep* **18**:1786–1800.

Gold VAM, Ieva R, Walter A, Pfanner N, Van Der Laan M, Kühlbrandt W. 2014. Visualizing active membrane protein complexes by electron cryotomography. *Nat Commun* **5**:4129.

Harner M, Neupert W, Deponte M. 2011. Lateral release of proteins from the TOM complex into the outer membrane of mitochondria. *EMBO J* **30**:3232–3241.

Hartl FU, Lecker S, Schiebel E, Hendrick JP, Wickner W. 1990. The binding cascade of SecB to SecA to SecY E mediates preprotein targeting to the E. coli plasma membrane. *Cell* **63**:269–279.

Horst M, Hilfiker-Rothenfluh S, Oppliger W, Schatz G. 1995. Dynamic interaction of the protein translocation systems in the inner and outer membranes of yeast mitochondria. *EMBO J* **14**:2293–2297.

Hoth M, Fanger CM, Lewis RS. 1997. Mitochondrial regulation of store-operated calcium signaling in T lymphocytes. *J Cell Biol* **137**:633-648.

Hwang S, Jascur T, Vestweber D, Pon L, Schatz G. 1989. Disrupted yeast mitochondria can import precursor proteins directly through their inner membrane. *J Cell Biol* **109**:487–493.

Koshkin V, Greenberg ML. 2002. Cardiolipin prevents rate-dependent uncoupling and provides osmotic stability in yeast mitochondria. *Biochem J* **364**:317.

Lill R, Stuart RA, Drygas ME, Nargang FE, Neupert W. 1992. Import of cytochrome c heme lyase into mitochondria: a novel pathway into the intermembrane space. *EMBO J* **11**:449–456.

Maarse AC, Blom J, Grivell LA, Meijer M. 1992. MPI1, an essential gene encoding a mitochondrial membrane protein, is possibly involved in protein import into yeast mitochondria. *EMBO J* **11**:3619–3628.

Maarsea AC, Blom J, Keilb P, Pfannerb N, Meijer M. 1994. Identification of the essential yeast protein MIM17, an integral mitochondrial inner membrane protein involved in protein import. *FEBS Lett* **349**:15–22.

Martin J, Mahlke K, Pfanner N. 1991. Role of an energized inner membrane in mitochondrial protein import: $\Delta\Psi$ drives the movement of presequences. *J Biol Chem* **266**:18051–18057.

Matouschek A, Azem A, Ratliff K, Glick BS, Schmid K, Schatz G. 1997. Active unfolding of precursor proteins during mitochondrial protein import **16**:6727–6736.

Mayer A, Lill R, Neupert W. 1993. Translocation and insertion of precursor proteins into isolated outer membranes of mitochondria. *J Cell Biol* **121**:1233–1243.

Neupert W, Brunner M. 2002. The Protein Import Motor of Mitochondria. *Nature Reviews Molecular Cell Biology* **3**:555-565

Neupert W, Herrmann JM. 2007. Translocation of Proteins into Mitochondria. *Annual Review of Biochemistry* **76:1**, 723-749

Nicholls DG. 1978. The regulation of extramitochondrial free calcium ion concentration by rat liver mitochondria. *Biochem J* **176**:463–474.

Nishikawa T, Edelstein D, Du XL, Yamagishi SI, Matsumura T, Kaneda Y, Yorek MA, Beebe D, Oates PJ, Hammes HP, Glardino I, Brownlee M. 2000. Normalizing mitochondrial superoxide production blocks three pathways of hyperglycaemic damage. *Nature* **404**:787–790.

Nowinski SM, Van Vranken JG, Dove KK, Rutter J. 2018. Impact of Mitochondrial Fatty Acid Synthesis on Mitochondrial Biogenesis. *Curr Biol* **28**:R1212-R1219

Ohba M, Schatz G. 1987. Disruption of the outer membrane restores protein import to trypsin-treated yeast mitochondria. *EMBO J* **6**:2117–2122.

Pereira GC, Allen WJ, Watkins DW, Buddrus L, Noone D, Liu X, Richardson AP, Chacinska A, Collinson I. 2019. A High-Resolution Luminescent Assay for Rapid and Continuous Monitoring of Protein Translocation across Biological Membranes. *J Mol Biol* **431**:1689–1699.

Ramesh A, Peleh V, Martinez-Caballero S, Wollweber F, Sommer F, Laan M van der, Schroda M, Alexander RT, Campo ML, Herrmann JM. 2016. A disulfide bond in the TIM23 complex is crucial for voltage gating and mitochondrial protein import. *J Cell Biol* **214**:417.

Rassow J, Guiard B, Wienhues U, Herzog V, Hartl FU, Neupert W. 1989. Translocation arrest by reversible folding of a precursor protein imported into mitochondria. A means to quantitate translocation contact sites. *J Cell Biol* **109**:1421–1428.

Rassow J, Hartl FU, Guiard B, Pfanner N, Neupert W. 1990. Polypeptides traverse the mitochondrial envelope in an extended state. *FEBS Lett* **275**:190–194.

Rouault TA. 2012. Biogenesis of iron-sulfur clusters in mammalian cells: New insights and relevance to human disease. *DMM Dis Model Mech* **5**:155-164

Martinez-Caballero S, Grigoriev SM, Herrmann JM, Campo ML, Kinnally KW. 2007. Tim17p regulates the twin pore structure and voltage gating of the mitochondrial protein import complex TIM23. *J Biol Chem* **282**:3584–3593.

Schendzielorz AB, Schulz C, Lytovchenko O, Clancy A, Guiard B, Ieva R, van der Laan M, Rehling P. 2017. Two distinct membrane potential-dependent steps drive mitochondrial

matrix protein translocation. *J Cell Biol* **216**:83–92.

Sirrenberg C, Endres M, Becker K, Bauert MF, Walther E, Neupert W, Brunner M. 1997. Functional cooperation and stoichiometry of protein translocases of the outer and inner membranes of mitochondria. *J Biol Chem* **272**:29963–29966.

Smith PK, Krohn RI, Hermanson GT, Mallia AK, Gartner FH, Provenzano MD, Fujimoto EK, Goeke NM, Olson BJ, Klenk DC. 1985. Measurement of Protein Using Bicinchoninic Acid. *Analytical Biochemistry* **150**:76-85

Ting SY, Yan NL, Schilke BA, Craig EA. 2017. Dual interaction of scaffold protein Tim44 of mitochondrial import motor with channel-forming translocase subunit Tim23. *Elife* **6**.e23609

Truscott KN, Kovermann P, Geissler A, Merlin A, Meijer M, Driessen AJM, Rassow J, Pfanner N, Wagner R. 2001. A presequence- and voltage-sensitive channel of the mitochondrial preprotein translocase formed by Tim23. *Nat Struct Biol 2001 812* **8**:1074–1082.

Tucker K, Park E. 2019. Cryo-EM structure of the mitochondrial protein-import channel TOM complex at near-atomic resolution. *Nat Struct Mol Biol* **26**:1158–1166.

Ungermann C, Guiard B, Neupert W, Cyr DM. 1996. The ΔΨ- and Hsp70/MIM44-dependent reaction cycle driving early steps of protein import into mitochondria. *EMBO J* **15**:735–744.

Vögtle FN, Wortelkamp S, Zahedi RP, Becker D, Leidhold C, Gevaert K, Kellermann J, Voos W, Sickmann A, Pfanner N, Meisinger C. 2009. Global Analysis of the Mitochondrial N-Proteome Identifies a Processing Peptidase Critical for Protein Stability. *Cell* **139**:428–439.

Wachter C, Schatz G, Glick BS. 1994. Protein import into mitochondria: the requirement for external ATP is precursor-specific whereas intramitochondrial ATP is universally needed for translocation into the matrix. *Mol Biol Cell* **5**:465–474.

Wang C, Youle RJ. 2009. The role of mitochondria in apoptosis. *Annu Rev Genet* **43**:95-118

Wurm CA, Jakobs S. 2006. Differential protein distributions define two sub-compartments of the mitochondrial inner membrane in yeast. *FEBS Lett* **580**:5628–5634.

1

Fig 1.

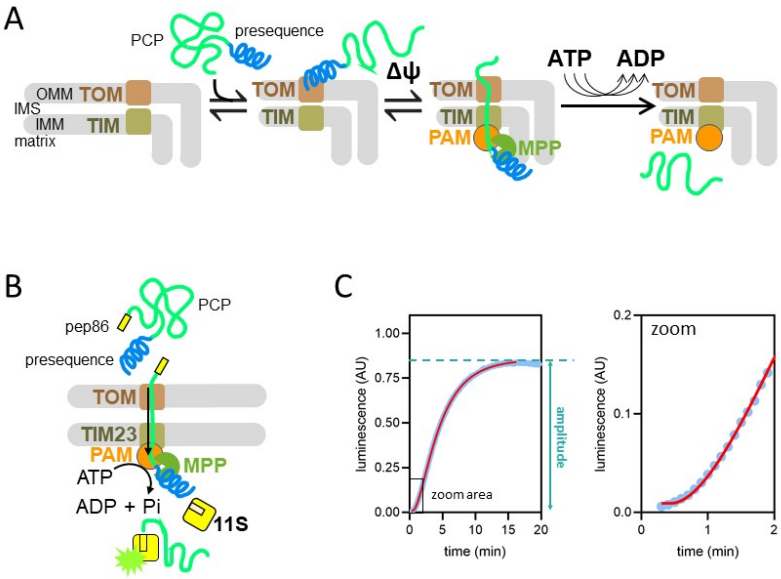

Fig 2.

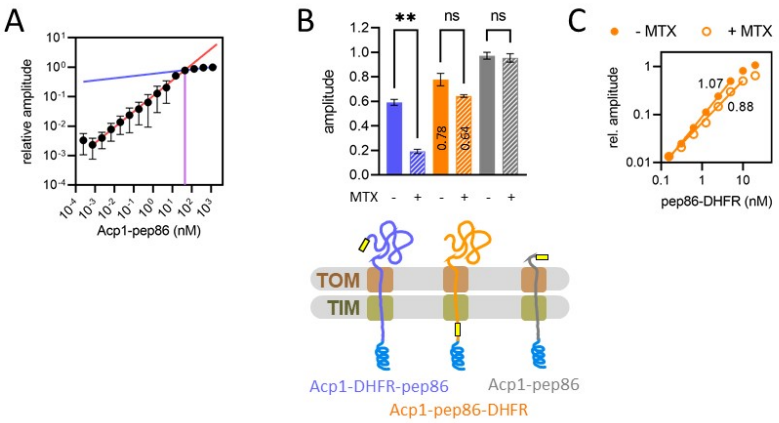

1

Fig 3.

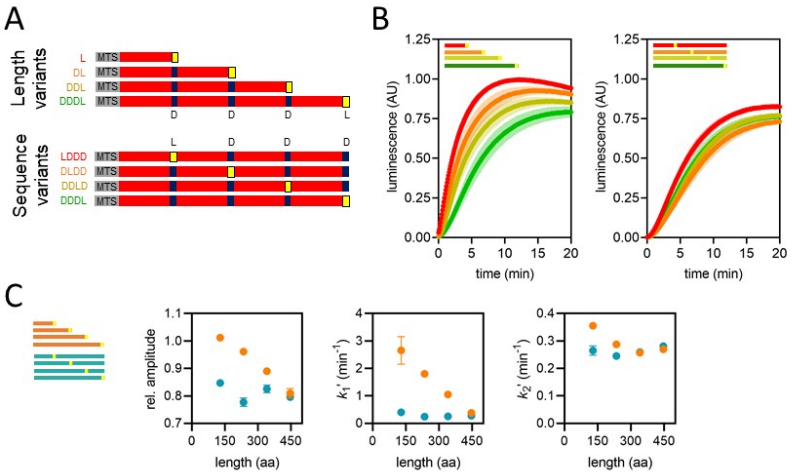

Fig 4

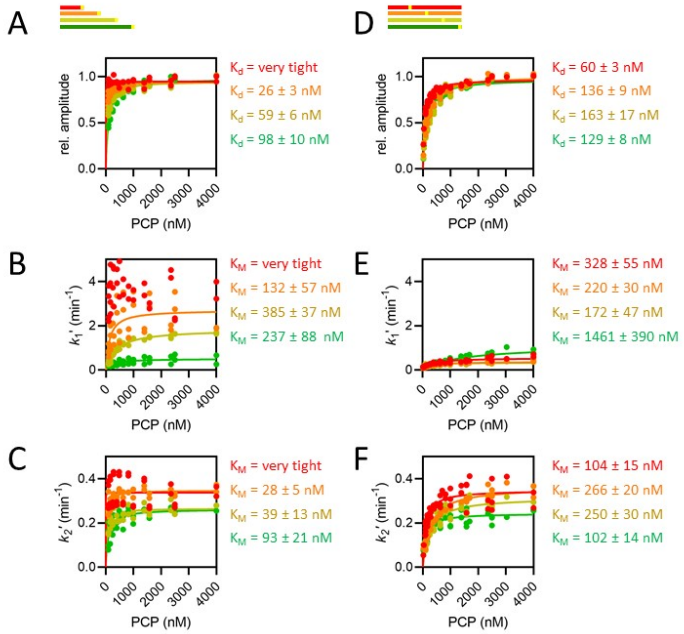

1

Fig 5.

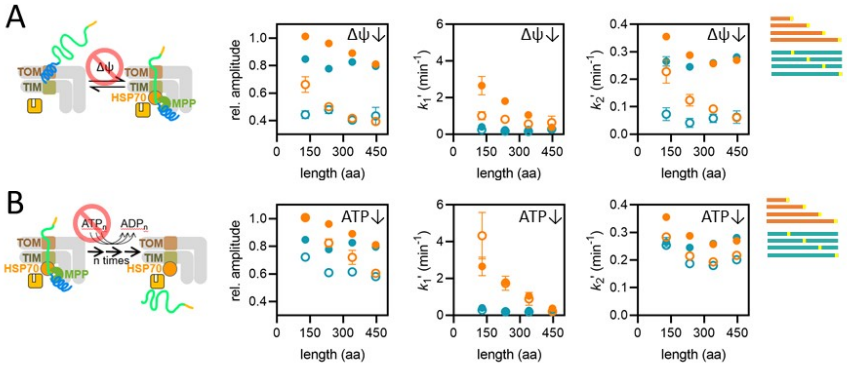

Fig 6.

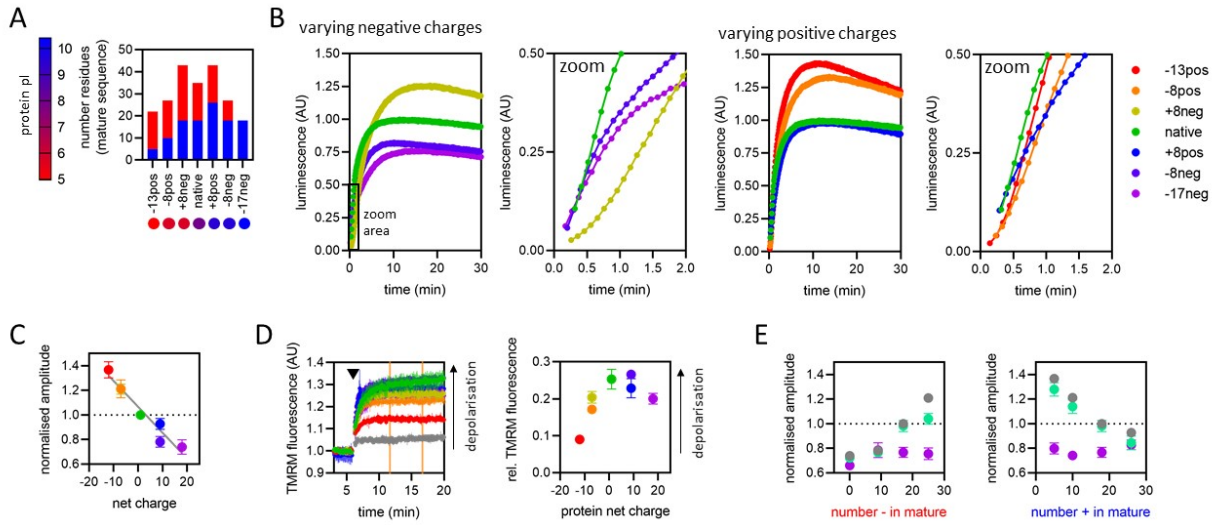

Fig 7.

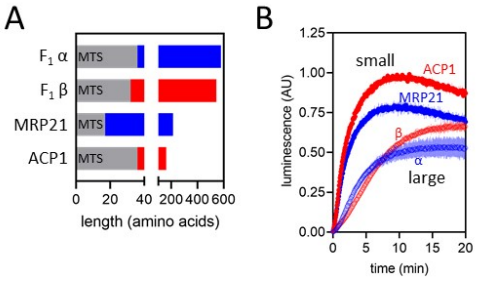

1

Fig S1.

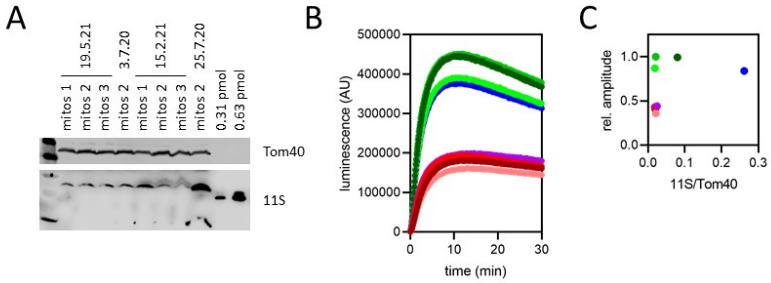

Fig S2.

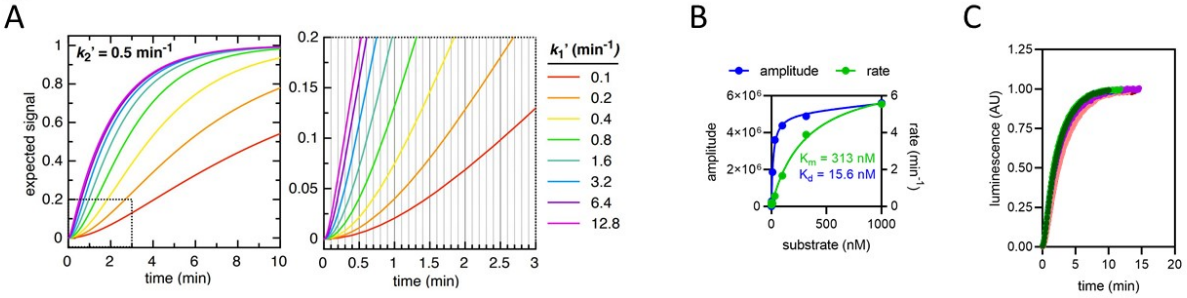

Fig S3.

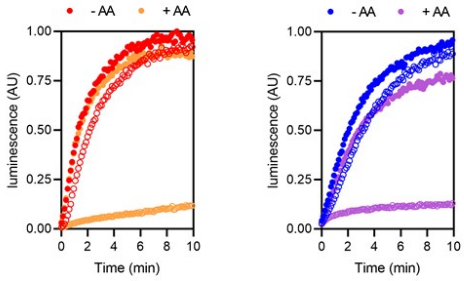

Fig S4.

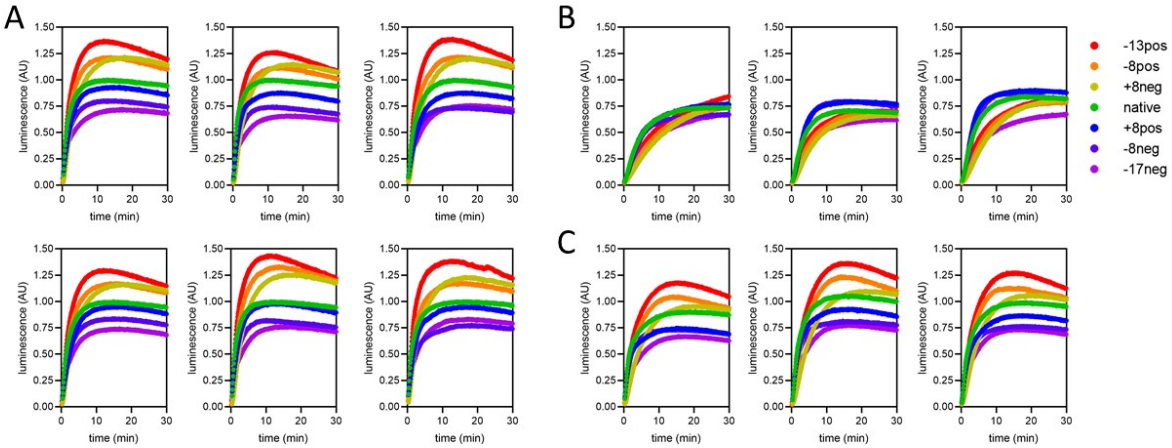

1